An Experimental Investigation into the Effect of Hydrodynamic Cavitation on Diesel

[*]R.D. Lockett, M. Jeshani

Department of Mechanical Engineering & Aeronautics, School of Engineering & Mathematical Sciences, The City University, Northampton Square, London EC1V 0HB, United Kingdom

Abstract

Samples of commercial diesel were subjected to forty hours of intense cavitation flow across a diesel injector in a specially designed high-pressure recirculation flow rig. Changes to the optical absorption and scattering properties of the diesel over time were identified by the continuous measurement of spectral extinction coefficients at 405 nm by means of a simple optical arrangement. Identical diesel samples were maintained at 70 ^{o}C for forty hours in a heated water bath, in order to distinguish the effects of hydrodynamic cavitation and temperature on the cavitated diesel samples.

The commercial diesel samples subjected to high pressure cavitation flow and water bath heating revealed a response to the flow and temperature history that was identified by an increase in the optical extinction coefficients of the cavitated and heated samples. The contribution of cavitation flow and temperature to the variation in spectral extinction coefficient was identified. It was concluded that the increases observed in the spectral extinction coefficients of the cavitated commercial diesels were caused by the cavitation affecting the aromatics in the commercial diesel samples.

* Corresponding Author: Email: r.d.lockett@city.ac.uk

Tel. 44 (0)207 040 8812

Fax. 44 (0)207 040 8655

Keywords

1. Introduction

Modern common rail direct injection diesel engines operate through the injection of high pressure liquid diesel fuel through magnetic solenoid actuated injectors directly into the engine cylinders. The diesel fuel is supplied to the injectors at high pressure from the common rail. When the fuel is supplied to the injectors, a proportion is injected into the engine, and the balance is returned to the fuel tank. If the engine is operated at low/part load, the rail pressure may be as low as 600 bar, and up to 40 % of the high pressure diesel supplied to the common rail and the injectors may be returned to the fuel tank via the fuel return pipes in the pump, common rail, and injectors [1]. However, when the engine is operated at high load, and depending on the engine, pump and common rail selected, the rail pressure may attain pressures of 1,400 bar to 2,000 bar. At these high load operating conditions, approximately 70 % to 80 % of the diesel supplied to the common rail and the injectors is injected into the engine, with the remainder being returned to the fuel tank.

The consequence of returning a significant fraction of the fuel supplied to the injectors back to the tank is that the proportion of diesel fuel subjected to repeated high pressure pumping is a substantial fraction of the original volume. This implies that a significant proportion of the diesel fuel has been re-circulated through the high pressure pump and rail and returned to the fuel tank, prior to admission to the engine.

In connection to this, fuel-derived deposits and sediments have been observed to develop at the entrance to, and inside the nozzle holes in modern mini-sac multi-hole diesel injectors [2, 3]. Indeed, deposits along the needle and on the needle seat have also been discovered [4].

These deposits are likely to have an impact on the internal flow and the external atomisation of the fuel jets emanating from the nozzle holes [5, 6].

Deposits at the exit of the injector nozzle holes may be formed through the partial oxidation and/or pyrolysis of liquid diesel located on the outer surface of the injector body, coming into contact with hot combustion gases originating in the cylinder [7, 8]. The mechanisms for deposit formation inside the nozzle holes, on the needle seat and along the needle are presently unknown.

Cavitation flow is believed to occur in high pressure diesel nozzles during diesel fuel injection, to significantly affect the structure and atomisation of the fuel jets emanating from the nozzles and entering the engine cylinders [9, 10]. Cavitation occurs when the diesel passes through or over a restriction, causing a large local pressure gradient and/or shear stress in the fluid. If the pressure gradient or shear stress in the fluid causes the local pressure to drop to less than the saturated vapour pressure at the local temperature, then the liquid may begin to boil locally, forming local pockets of diesel fuel vapour [11]. Cavitation is also thought to be capable of altering injector surfaces though local hydro-erosion and hydro-grinding [12]. In extreme circumstances, cavitation may cause injector failure [13]. It has been observed directly in a number of diesel fuel injection experiments [14 - 16].

There is anecdotal evidence that cavitation flow occurs inside automotive diesel common rail pumps during high pressure pumping [17, 18]. Hydrodynamic cavitation is likely to occur near the high pressure cylinder valves in the pump, and in the fuel return valves located in the pump, common rail, and the injectors. In addition, there is a trend within the diesel fuel injection equipment (FIE) industry towards increasing common rail pressures. Indeed, Bosch

has developed a 2,500 bar common rail fuel injection system [19], while both Denso and Delphi Diesel Systems have reported the development of 3,000 bar common rail diesel fuel injection systems [20, 21].

The industry trend towards larger common rail pressures may begin to affect the diesel fuel subjected to such extreme conditions, during pumping, storage and in flow. This may occur through pyrolysis and/or intense cavitation flow, causing chemical re-arrangement and decomposition. This may, in turn, lead to deposit formation (sedimentation) and ultimately, to equipment failure.

The effect of cavitation on alkanes was first investigated by Suslick *et al*. [22]. They employed high intensity ultrasound on alkane solutions, and discovered primary products of hydrogen, methane, acetylene, and smaller 1-alkenes. They suggested that the reactions in the system bore strong similarities to high temperature pyrolysis, and concluded that the principal sono-chemical process responsible was C-C bond cleavage with secondary abstractions and re-arrangements. This was considered to be the consequence of high temperature regions developing in the multi-phase solution as a result of cavitation bubble collapse.

The corresponding effects of ultrasound cavitation in diesel has been investigated by Price *et al*. [23, 24]. They employed high intensity ultrasound to irradiate a diesel fuel sample, and observed the decomposition of saturated alkanes, and identified sonically promoted polymerization reactions that led to aromatics forming insoluble sediments (gums), similar to those reported by Pedley *et al*. [25] and Kalitchin *et al*. [26] as a result of the long term storage of diesel.

These investigatory reports [22 - 24] represent a small subset of the growing number of investigatory reports into ultrasonic sono-chemistry in liquids. This is a recently developing field of chemistry, which involves theoretical, modelling and experimental research into the acceleration of reaction rates involving chemical reactions in liquid suspensions, solutions and/or pure liquids through the use of intense ultrasound [27]. It is believed that intense ultrasonic excitation of a suspension, solution or pure liquid induces the formation and collapse of many energetic micro-bubbles within the liquid, which are thought to develop very large internal vapour temperatures and pressures during bubble collapse. This process is known as ultrasonic cavitation, or ultrasound induced cavitation. The large internal vapour temperatures achieved during cavitation bubble collapse may lead to molecular decomposition and even plasma formation [28]. Indeed, Suslick *et al.* have reported internal bubble temperature measurements of up to 5,000 K occurring during ultrasonic cavitation bubble collapse [29].

These observations in ultra-sound cavitation of diesel raise the question of whether similar effects occur, and are observable in hydrodynamic cavitation of diesel. Furthermore, it is necessary to discover whether high pressure diesel common rail fuel injection equipment produce hydrodynamic cavitation internally, and whether any such cavitation induces sono-chemistry effects on the diesel fuel, resulting in deposit formation (sedimentation), similar to that reported earlier.

It was therefore considered necessary to investigate the conditions that exist in high pressure pumping systems, and their effect on the physical and chemical stability of the diesel fuel (through an analysis of the variation of the physical and chemical properties and composition of the fuel).

The aim of this work was to establish whether hydrodynamic cavitation introduced alterations to the diesel that could be identified using a simple measurement technique. This led to the design and manufacture of a high pressure, continuous re-circulation, cavitation flow rig that produced intense hydrodynamic cavitation flow continuously, involving a moderate volume of re-circulating diesel. A simple measurement technique for the identification and determination of change in composition and rate of change of composition of the diesel sample was required to be developed.

In this regard, the measurements and observations reported in Suslick *et al.* [22] and Price *et al*. [23, 24] suggest that ultrasonic cavitation in diesel produces pyrolysis and the formation of insoluble sediments. Pyrolysis reactions in diesel necessarily result in the formation of primary soot particles (1 nm - 10 nm diameter), which are then able to aggregate to form larger soot particles (100 nm - 10 μm), or bind to other particulates to form other sediments [30]. Both of these sets of findings and observations suggest the formation and development of soot-like particle suspensions in the diesel fuel samples. These lead to two significant hypotheses: (1) hydrodynamic cavitation of diesel will produce similar observable effects to those produced by ultrasonic cavitation (suggesting that the mechanisms for inducing the pyrolysis sono-chemistry in the diesel samples are similar), and (2) the formation of a particulate suspension in the diesel will be detectable using a simple optical extinction measurement system.

The second hypothesis led to the development of a simple optical extinction measurement system, intended to identify and determine variations in the spectral extinction coefficients of the diesel samples as a result of changes in the composition of the samples, and/or the

7

formation and development of particle suspensions in the samples, arising out of cavitation induced diesel fuel pyrolysis.

The optical extinction measurement system developed and employed in these experiments was a simplification of the spectral extinction and scattering method [31, 32]. This method is used widely in the determination of particle properties in suspensions, colloids and aerosols [33, 34]. It is also employed in the determination of real and imaginary refractive indices in absorptive media [35, 36].

A number of commercial and non-commercial diesel samples were subjected to continuous cavitation flow and exposure to a hot water bath in the course of the experimental work reported here. The results obtained from four commercial diesel samples and a non-commercial, model diesel sample are reported and discussed in this paper. The four commercial diesel samples discussed here consisted of two newly bought samples, and two samples that had been stored separately in diesel storage tanks for a year. The model diesel sample tested was comprised of a paraffin blend (> 98 % paraffins), containing zero aromatics.

The hot water bath was employed in order to separate out the combined effects of cavitation and the release of internal compression energy during the diesel flow through the diesel nozzle into the receiver. This was in order to identify and separate out the effects of temperature and cavitation on the diesel samples.

The paper is structured to introduce the reader to the design features and use of the experimental equipment designed and manufactured for this study. This is followed by a

detailed description of the experimental method employed in the study, together with a description of the layout and calibration of the optical extinction measurement system. This is accompanied by a presentation of the results, a discussion of the main findings, and the conclusion.

2. Experimental Equipment

2.1 The High Pressure, Continuous Re-Circulation, Cavitation Flow Rig

A high pressure, continuous flow rig was designed in order to ensure continuously re-circulating flow of high pressure diesel fuel through a permanently open diesel injector nozzle into a low pressure receiver. A simplified schematic of the rig is shown in Figure 1. Diesel fuel was supplied from a small fuel tank to a low pressure feed pump, which fed the diesel through a 5 μm nylon fuel filter to a fixed displacement, five cylinder, high pressure pump (Dynex PF1318H-10) with a delivery pressure of 1.3 bar. The Dynex pump was connected to a 4.2 kW variable speed electric motor by a shaft, which provided the pump with the power and torque necessary to pump the diesel around the re-circulating system. The Dynex pump had a case volume of 150 cm^3, and was capable of providing flow rates of up to 3.80 l/min, at pressures of up to 630 bar, when driven by the motor at 1,800 rpm [37]. The diesel fuel pressure in the high pressure tubing was measured using a conventional pressure gauge. The minimum volume of diesel to be re-circulated in the cavitation flow rig was 3.5 litres.
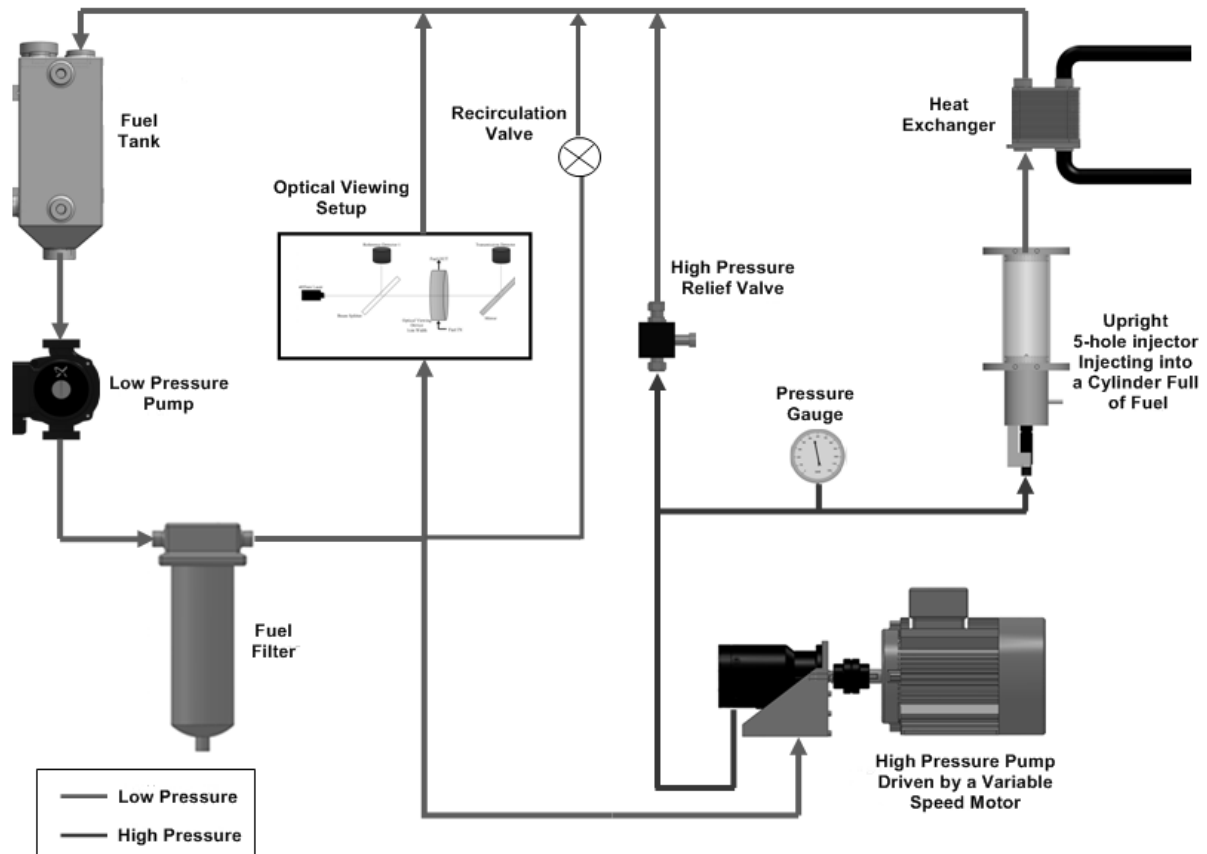
Figure 1: Schematic of Continuous, High Pressure, Cavitation Flow Rig

The Dynex pump continuously supplied high pressure diesel (preset to 550 bar $\pm$ 10 bar) to a permanently open 0.22 mm diameter five-hole asymmetric diesel nozzle (Bosch diesel nozzle Part Number DSLA148P591 with needle removed). The diesel injector nozzle released the diesel fuel into a 1.0 litre receiving cylinder maintained at atmospheric pressure. The continuous re-circulation of fuel through the high pressure pump and diesel nozzle caused the temperature of the diesel to rise to dangerous levels. Consequently, a temperature control system was installed in order to maintain the temperature of the diesel in the re-circulating flow rig at a safe, constant value. The temperature control system utilised a control thermocouple, a commercial temperature controller, and a heat exchanger. The control thermocouple was attached to the high pressure tubing upstream of the open diesel injector,

and communicated the pre-expansion diesel temperature to the temperature control system. The temperature control system controlled the temperature of the diesel by controlling the water supply to a compact, helical, rectangular plate counter-flow heat exchanger, located immediately downstream of the receiver. Once the diesel had passed through the heat exchanger, it was returned to the fuel tank. Two additional thermocouples were located (1) near the entrance to the high pressure pump, and (2) on the main return pipe to the fuel tank, in order to monitor the temperature of the diesel fuel samples elsewhere in the system.

A safety pressure relief valve providing an over-pressure fuel return to the tank was installed between the high pressure pump and the diesel injector in order to relieve the pump and tubing of over-pressure conditions and/or high pressure surges. The pressure relief valve was manually set to relieve the diesel in the high pressure tubing at 630 bar and above.

2.2 The Optical Extinction Measurement System

The objective here was the development of a simple, sensitive experimental technique, to be used for the determination of the change in composition of the diesel samples subjected to re-circulating cavitation flow in the high pressure rig.

This consideration led to the hypothesis that a change in the composition of the diesel fuel samples would lead to a corresponding change in the spectral extinction coefficients of the diesel samples, through the destruction of optically active molecular species comprising the diesel samples, and the formation of new optically active molecular species. The long term cavitation in the high pressure flow rig might also result in the formation of carbon-rich

particles, which would produce a corresponding increase in the spectral extinction coefficients of the diesel fuel samples.

The extinction measurement system described here is a simplification of an extinction-scattering measurement system, usually employed to determine sample refractive index, and scattering and extinction coefficients. Extinction-scattering measurement systems usually determine the extinction length and the amount of incident light scattered from the optical path by the scattering system. The extent of the absorption and scattering of the incident light is specified by the Beer-Lambert-Bouguer Law

$$I_t(x) = I_0 e^{-\alpha x}, \tag{1}$$

where I_0, x and $I_t(x)$ are the spectral flux of light incident on an absorptive sample, the distance the light travels through the sample, and the spectral flux after travelling distance x respectively. α is termed the spectral extinction coefficient, and is comprised of the scattering coefficient α_{sc} and the absorption coefficient α_{abs} i.e. $\alpha = \alpha_{sc} + \alpha_{abs}$. The extinction coefficient α is related to the complex refractive index of the sample (specified by $n = m + ik$) by the relation

$$\alpha = \frac{4\pi k}{\lambda} = \frac{4\pi}{\lambda} Im(n) \tag{2}$$

where λ is the wavelength of the incident light [38].

In these experiments, the overall refractive index of the diesel samples is comprised of the overall refractive index of the blend of aliphatics, aromatics and additives making up the

liquid content, taken together with the overall refractive index of any particles in suspension. The overall extinction coefficient can be expressed in terms of a sum over the respective scattering and absorption terms

$$\alpha = \alpha_{sc} + \alpha_{abs} = \alpha_{sc}^{(l)} + \alpha_{sc}^{(p)} + \alpha_{abs}^{(l)} + \alpha_{abs}^{(p)} \qquad (3)$$

where $\alpha_{sc}^{(l)}$, $\alpha_{abs}^{(l)}$, $\alpha_{sc}^{(p)}$, and $\alpha_{abs}^{(p)}$ are the scattering and absorption coefficients for the liquid and the particle suspension respectively.

2.2.1 The Optically Accessible Cell

Continuous sampling of a fraction of the re-circulating diesel was undertaken, by connecting a sampling tube to the main diesel fuel tube connecting the fuel filter to the suction port of the high pressure Dynex pump. The sampling tube continuously supplied a small flow of diesel to an optically accessible cell, and then returned it from the cell, back to the fuel tank. A schematic of the optically accessible cell in shown in Figure 2.

The optically accessible cell consisted of a short hollow stainless steel cylinder 20 mm wide, 80 mm diameter with a wall thickness of 30 mm. A 5 mm deep, 40.1 mm diameter recess was bored into both ends of the cylinder, providing the space for 40 mm diameter windows. Six M6 bolt holes were symmetrically placed on the outer faces of the main cylinder near the outer edges, and threaded. Two stainless-steel cylindrical disc end plates containing six M6 size bolt holes were manufactured in order to locate, hold and seal the fused silica windows in place, using four polypropylene gaskets to protect and seal the windows. 5mm thick, 40

13

mm diameter uv grade fused silica windows were then located and sealed against the gaskets, which were located against the recessed flanges of the main body of the cell. The windows were clamped to the cell by screwing down the end-plates using M6 bolts, forming a sealed volume in the centre of the cell.
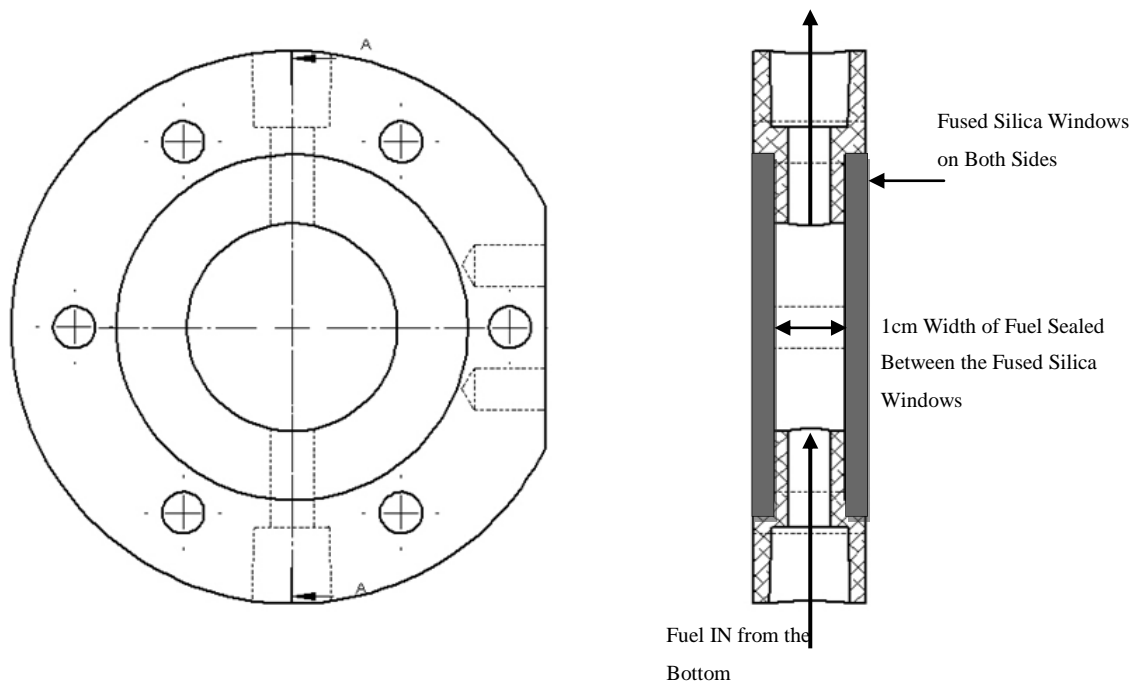

Fused Silica Windows on Both Sides

1cm Width of Fuel Sealed Between the Fused Silica Windows

Fuel IN from the Bottom

Figure 2: Schematic of Optically Accessible Cell

Fuel access ports on opposite sides of the cylinder were radially drilled through the cylinder wall, providing flow access into the central volume. Flexible braided hoses transported the sampled diesel from the rig to the port at the bottom of the optically accessible cell. The diesel then flowed up the port, filling the 1 cm wide, 4 cm diameter cylindrical space in the cell, before flowing upwards into the return hose, returning the sampled diesel back to the fuel tank.

2.2.2 The Laser Measurement System

A 405 nm laser beam (originating from a World Star Tech. 405 nm diode laser) was directed through a 0.03 OD neutral density filter (50 mm x 50 mm uv grade fused silica glass sheet) placed at 45° to the incident beam, before being passed through the optically accessible cell containing the sampled diesel flowing from the rig and back to the fuel tank. The fraction of the beam reflected from the angled neutral density filter was directed onto a Laserpoint laser power detector in order to obtain a reference laser power. The main laser beam passing through the optically accessible cell was attenuated as a result of optical absorption and scattering from the 1 cm wide diesel fuel sample flowing through the cell, and scattering from the two fused silica windows. The attenuated beam leaving the cell was then directed onto a mirror, which reflected the beam onto a second Laserpoint laser power detector. Figure 3 shows the assembly of the laser, neutral density filter, optically accessible cell, mirror and laser power meters.
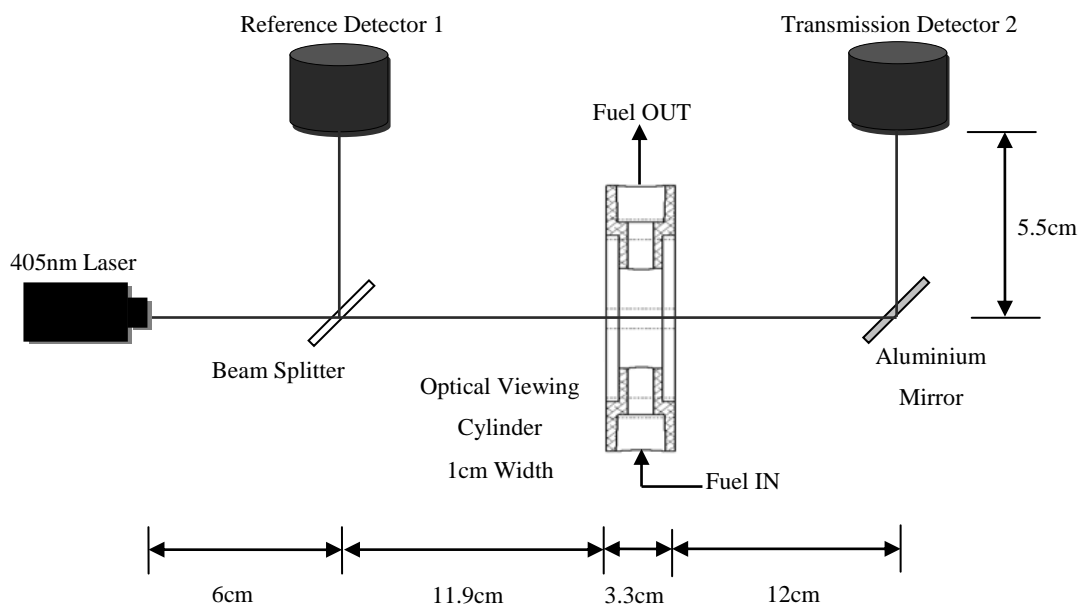

Figure 3: Optical Layout for Laser Extinction Measurement in Diesel

Both of the Laserpoint laser power detectors utilized a USB interface to record the measured laser power on a computer using PC-Link software. The control program provided the user with the ability to calibrate the power detectors under different lighting conditions prior to measurement. The software provided a 10 x gain function in order to increase the sensitivity of the detectors, making them capable of determining laser power from 10 µW to 200 mW in discrete intervals of 10 µW.

2.3 The Water Bath

A 20 litre commercial tea urn was fitted with a level gauge and a K-type thermocouple. A custom built temperature control box enabled the temperature of the water filling the urn to be set and controlled with an uncertainty of $\pm$ 0.5 ^{o}C. This was achieved in a simple manner by the temperature control system, which compared the measured temperature against the set temperature, and turned the 240 V ac electrical supply to the urn element on and off, depending on the variation of the water temperature from the set temperature.

Bottle platform stands were manufactured in order to place a 2.5 litre laboratory glass bottle and a 1 litre laboratory glass bottle in the urn, in order for the diesel samples in the bottles to be fully immersed in the water, but with the bottle tops and caps maintained above the water line. The bottle caps were drilled and fitted with breathing ports and tubing, which facilitated pressure equalization and ventilation during immersion in the water bath. Figure 4 shows the urn and platform stand assembly.
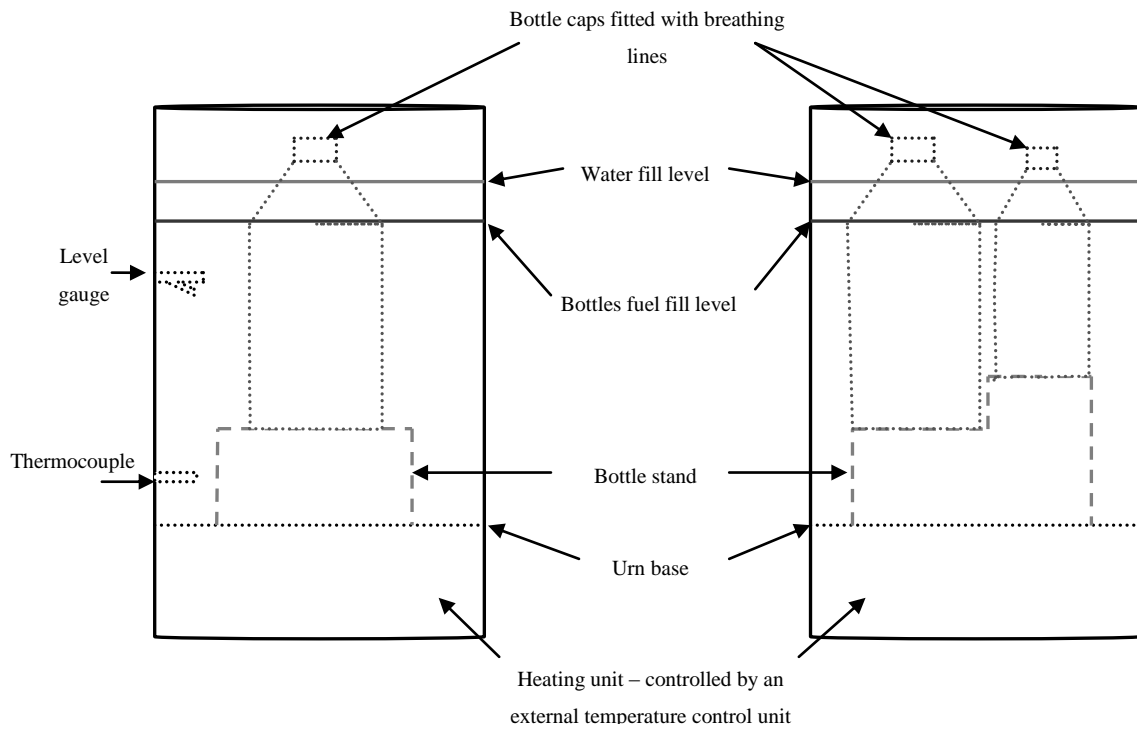
Bottle caps fitted with breathing lines

Water fill level

Bottles fuel fill level

Level gauge

Thermocouple

Bottle stand

Urn base

Heating unit – controlled by an external temperature control unit

Figure 4: Schematic of Modified Tea Urn, Platform, and Bottle Assembly

3. Experimental Method

3.1 Re-Circulation Flow Tests in the High Pressure Cavitation Rig

Before a new fuel test, the high pressure flow rig was flushed twice with 3.5 litres of 95 % grade hexadecane (supplied by Alfa-Aesar), followed by filling the system with 3.7 litres of the diesel sample that was to be tested. The flushing process consisted of filling the fuel tank slowly with the flushing liquid while the low pressure feed-pump was being run. Once the receiving cylinder began to receive flushing liquid from the diesel nozzle (indicating that the lower part of the system was filled with liquid), the high pressure pump was started, and driven by the motor to produce a pressure of 300 bar. This served to fill the receiving cylinder and the heat exchanger, before returning the fuel to the main fuel tank. Once the

components were filled, the flushing liquid was circulated around the system at 300 bar and 50 °C for approximately one hour.

Between successive tests and flushes the system was drained. Four drain valves were used to drain the rig of diesel or flushing liquid. The first drain valve was attached to the base of the filter housing, and was employed to drain the tank, low pressure pump, filter, and a fraction of the high pressure pump. Approximately 2.2 litre of liquid was drained from the first drain valve. The second drain valve was located at the base of the receiving cylinder, which was employed to drain the receiving cylinder and the heat exchanger. Bottle nitrogen was employed to provide back pressure to the heat exchanger in order to ensure that the heat exchanger was fully drained. Approximately 0.5 litres of liquid was drained from the second drainage point. Liquid was then drained from the high pressure exit near the diesel nozzle, and from the low pressure entry to the high pressure pump. Approximately 0.4 litres of liquid was drained from these two points. Therefore for each fill of 3.5 litres of diesel or hexadecane flushing liquid, approximately 3.2 litres was able to be drained. This left approximately 300 ml in the system in the form of residual volume from the previous test or flush. A full test cycle consisting of two flushes and a new test fuel fill resulted in a test cycle to test cycle contamination of the order of 0.1 %.

Once the rig was filled with approximately 3.7 litres of a new test fuel (using the procedure specified earlier), it was circulated around the rig for approximately 30 minutes at low pressure. During this period the laser power detectors were calibrated for the local light level. A 200 ml pre-test sample was then drawn off from the filter drain valve, providing a reference pre-test sample for later chemical analysis.

The pre-injection temperature was initially set to 55 ^{o}C. The low pressure pump was then turned back on, allowing the remaining 3.5 litre test diesel sample in the rig to circulate at low pressure. The laser was turned on, and allowed to settle, before a laser power reading was taken from both detectors. The high pressure pump was then turned on, and the motor speed and the pressure upstream of the diesel nozzle slowly increased to 550 bar. The continuous release of the compression energy during diesel flow through the nozzle into the receiver resulted in a temperature rise. Once the temperature reached 55 ^{o}C, one full temperature cycle was allowed, before setting the temperature control point to its test value of 70 ^{o}C. The temperature continued to rise until the set point was achieved, at which time the temperature control system began supplying cold water to the heat exchanger, maintaining the diesel pre-injection temperature at 70 ^{o}C $\pm$ 2 ^{o}C.

The compression energy transferred from the high pressure pump to the diesel fuel samples during compression resulted in a temperature rise of approximately 15 ^{o}C in the downstream high pressure diesel relative to the upstream low pressure diesel. The further dissipation of compression energy released during the expansion flow though the nozzle, the formation and development of cavitation flow in the nozzle and receiver, and the dissipation of turbulence energy resulted in a further 25 ^{o}C temperature rise in the receiver. This is to be compared with a total theoretical temperature rise of 42 ^{o}C ($\Delta T \approx \Delta p/\rho c$, where ΔT, Δp, ρ and c are the theoretical temperature rise, the pressure rise in the pump, the diesel fuel density, and the diesel specific heat respectively).

The diesel test sample was circulated around the system for ten hours per day, for four successive days, for a total of forty hours cavitation test time. During the cavitation flow tests, the laser detectors were sampling the reference and transmitted laser power with a

sampling rate of 1 Hz. The computer control software computed a one minute average of the discrete reference and transmitted laser power measurements, and then wrote the one minute laser power averages to a text file for later analysis. The one minute laser power averages for the reference and transmitted beams were recorded continuously over the ten hour cavitation test period. At the end of the ten hour period the electric motor and pump were slowed down to a stop, and the diesel test sample allowed to cool. The following day the standard run procedure was repeated, and this was undertaken for four successive days.

Four commercial diesel samples and one model diesel sample were subjected to forty hours continuous cavitation and water bath heating tests. Two of the four commercial diesel fuel samples were stored, and then tested within three months of purchase. The other two commercial samples were stored for between twelve and fifteen months prior to testing. The model diesel sample was comprised of a blend of C_{10} to C_{19} paraffins (> 98 %).

3.2 Water Bath Tests

Before the diesel samples were immersed in the hot water bath, pre-bath laser transmission tests were undertaken. The cavitation flow rig was filled with the diesel sample to be tested, and circulated around the system and through the optically accessible cell at ambient temperature using the low pressure pump. The diode laser was turned on, and the beams directed onto the reference detector, and through the optical cell, and onto the transmission detector. The reference laser power and transmitted laser power incident on the detectors were recorded for approximately 15 minutes circulation time.

Two types of water bath tests were then undertaken. The first test involved an attempt to reproduce the temperature history achieved in the cavitation flow tests. 3.5 litre of fresh diesel fuel sample were immersed in water, maintained at 70 $^\circ$C, for ten hours per day for four days. The second test involved the immersion of fresh 3.5 litre diesel samples in water at 70 $^\circ$C for a continuous, uninterrupted period of forty hours.

After the hot water immersion tests were complete, the cavitation flow rig was filled with the post-immersion diesel samples, and circulated around the rig and through the optically accessible cell at ambient temperature. Reference and transmitted laser power was again recorded, in the same manner as identified earlier. The diode laser was turned on, and the beams directed onto the reference detector via the neutral density filter, and through the optical cell, and onto the transmission detector. The reference laser power and transmitted laser power incident on the detectors were recorded for approximately 15 minutes circulation time.

3.3 Analysis and Calibration of the Laser Detection System

3.3.1 Analysis of the Spectral Extinction Coefficient

The 405 nm laser beam transmitted through the diesel samples was subject to internal absorption and scattering. The transmitted laser power is expressed in terms of the Beer-Lambert-Bouguer Law for optical extinction

$$I_t(x) = I_0 e^{-\alpha x}, \tag{4}$$

where I_0 is the initial laser power incident on the diesel sample, and $I_t(x)$ is the transmitted laser power at point x in the sample, after having traversed a distance x through the sample. As identified earlier in Equation (1), α is the spectral extinction coefficient, and is comprised of the spectral absorptivity α_{abs}, and the spectral scattering coefficient α_{sc}, i.e. $\alpha = \alpha_{abs} + \alpha_{sc}$.

The laser power incident on the diesel samples I_0 has to pass through the reference beam filter, followed by the fused silica window into the optical cell, i.e $I_0 = t_f t_{fs} I_{laser}$, where t_f, t_{fs} and I_{laser} are the transmission factor through the OD0.03 neutral density filter, the transmission factor through a fused silica window, and the 405 nm diode laser power respectively. I_0 can also be expressed in terms of the laser power reflected from the neutral density filter onto the reference laser power detector I_{ref} (reference detector laser power).

$$I_0 = \frac{t_{fs}(1-r_f)}{r_f} I_{ref} \qquad (5)$$

where t_{fs} is as before, and r_f is the reflectivity of the OD0.03 neutral density filter, being used as a beam-splitter.

The laser power exiting the diesel samples pass through a fused silica window before being reflected from a 45° angled mirror onto the transmission laser power detector. The laser power measured with the detector is denoted by I_P, and is related to the laser power exiting the diesel sample in the optical cell I_t by

$$I_P = t_{fs} r_m I_t, \qquad (6)$$

where t_{fs} is the transmission coefficient for the exit fused silica window (as defined above), and r_m is the reflectivity of the final mirror. The time-dependent spectral extinction coefficient is then derived from equation (1) to be

$$\alpha(t) = \frac{ln\frac{I_0(t)}{I_t(t)}}{l} = \frac{ln\frac{t_{fs}^2 rm\left(1-r_f\right)I_{ref}(t)}{r_f I_P(t)}}{l} \qquad (7),$$

where l is the optical path length of the laser through the diesel in the optical cell. The optical path length in the cell was measured to be 1.03 cm $\pm$ 0.01 cm.

3.3.2 Calibration of the Optical Extinction System

Each optical element affecting the laser detection system was independently investigated and calibrated. The calibration of the system began with the direct measurement of the un-attenuated diode laser beam power by directing the diode laser beam directly onto the transmission power meter. Average power measurements of the un-attenuated laser beam were obtained, and stored on the pc.

The first optical element to be investigated was the OD 0.03 fused silica neutral density (ND) filter placed at 45° to the incident laser beam. The optical arrangement is shown in Figure 5 below. During the cavitation flow experiment, it was employed to reflect approximately 10% of the incident diode laser beam towards the reference laser power meter, while allowing the balance of the beam to pass through the filter towards the optically accessible cell. A number of neutral density filters were employed to attenuate the beam originating from the diode laser, and were located between the diode laser and the angled neutral density filter.
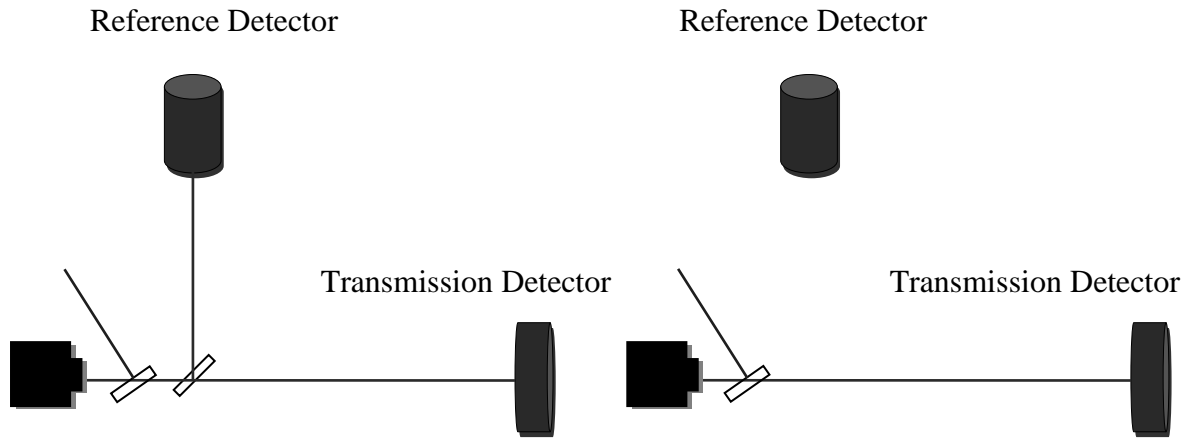
Figure 5: Optical Layout for the Calibration of the Beam-splitter

Nine average reflected beam power measurements were obtained from the reflected beam falling on the reference power meter (denoted by I_{ref}) and transmitted beam power measurements were obtained from the transmitted beam falling on the transmission power meter (denoted by I_{T2}), for three different attenuations (four including the origin). The graph is shown in Figure 6. A linear plot of I_{T2} as a function of I_{ref} including the origin produced the proportional relationship $I_{T2} = 9.031 I_{ref}$, with a linear correlation coefficient of $R^2 = 0.9982$. A comparison between the values of I_{T2} derived from the proportional relationship with the measured values produced a mean relative error of 0.8 %. This means that the neutral density filter reflected 0.099 ± 0.001 of the incident laser power onto the reference detector.

The second set of optical elements to be calibrated were the fused silica windows that were employed to provide optical access to the diesel samples and to seal the optical cell. The optical transmission through the fused silica windows had to be calibrated with a transparent fluid flowing though the optical cell during the calibration measurements, with the transparent fluid having a refractive index matching those of the diesel samples. This was in

order to calibrate the effect of the laser passing from the entrance fused silica window into the diesel sample, to be followed by the laser exiting the diesel, and entering the exit fused silica window.
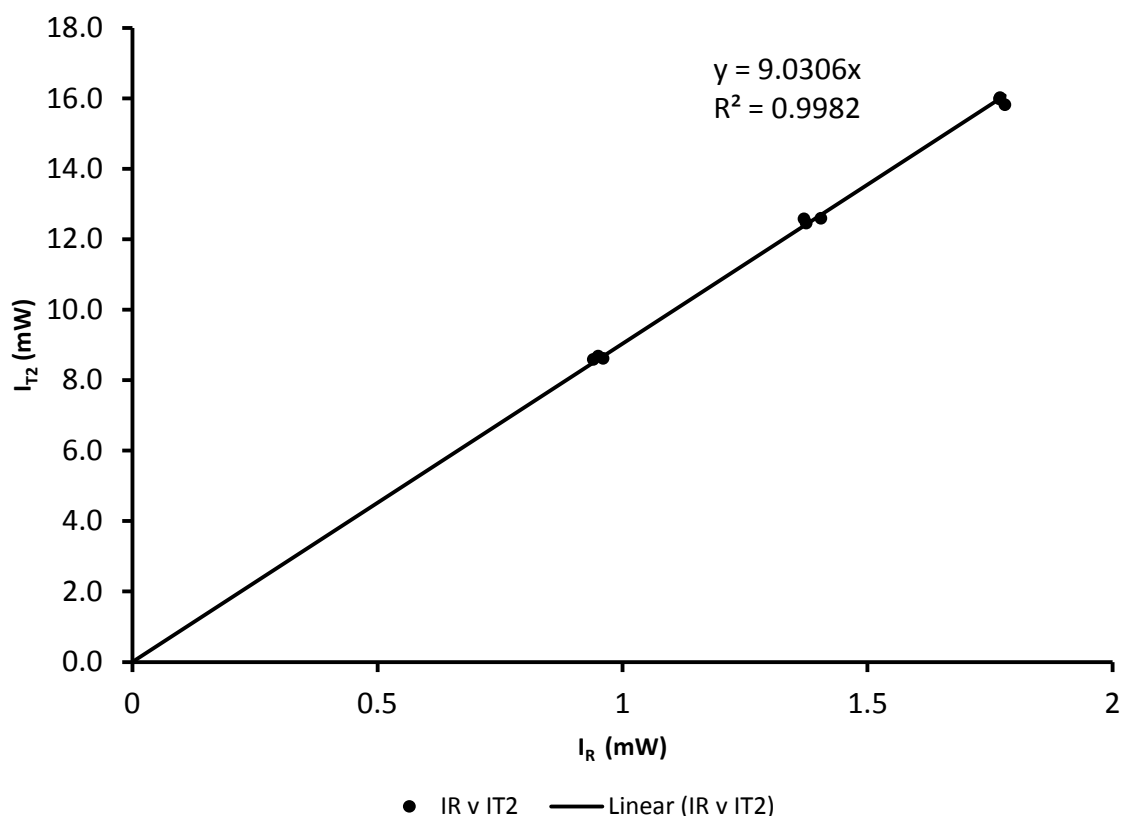

Figure 6: Graph of Transmitted Laser Power (mW) as a Function of Reflected Laser Power (mW)

A C_{10} to C_{19} paraffin blend was employed as a model diesel in order to calibrate the optical transmission of the laser through the fused silica windows sealing the optically accessible cell. The paraffin blend was almost transparent to the diode laser light at 405 nm. Figure 7 shows a schematic of the experimental arrangement necessary to calibrate the transmission through the fused silica windows.
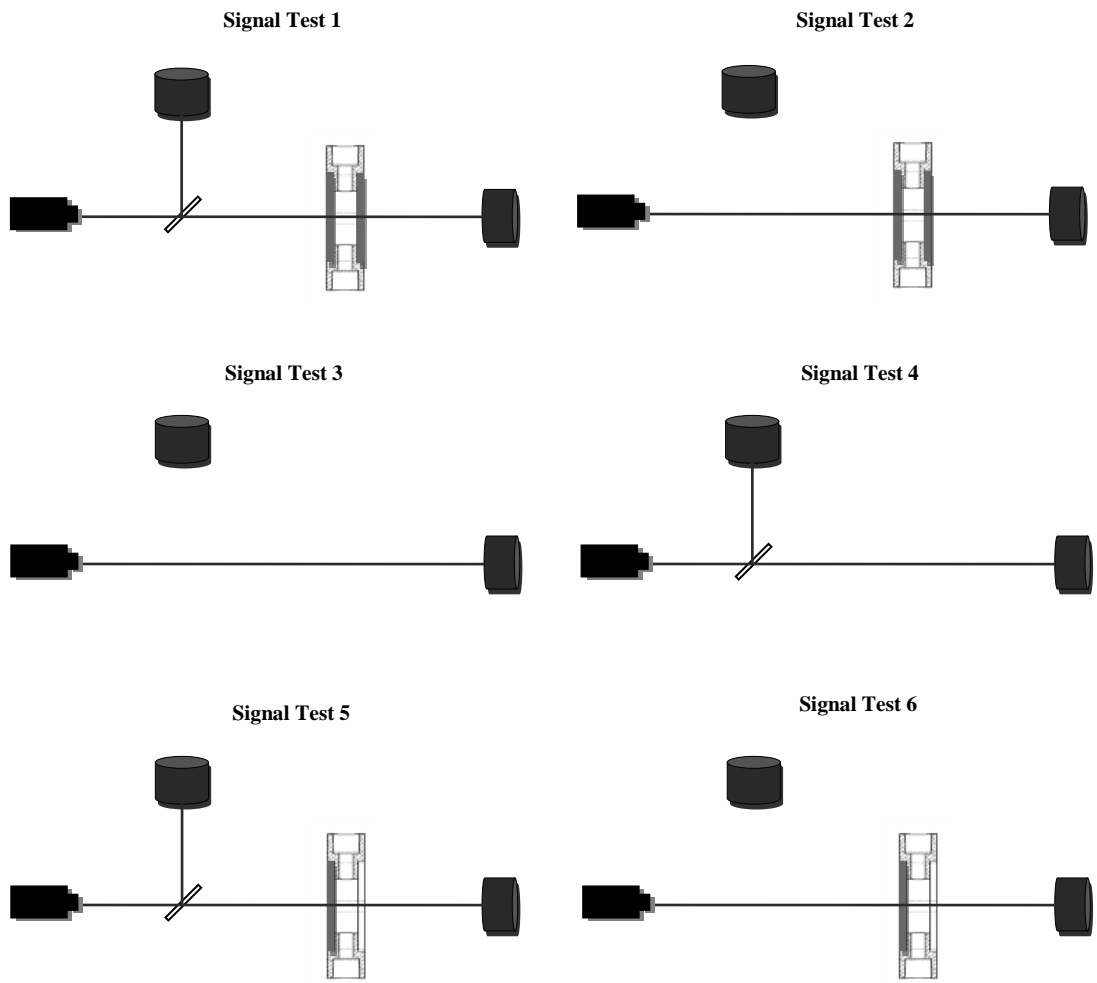
Figure 7: Optical Layout for the Measurement of Transmission through Fused Silica Windows

The transmission through the fused silica windows were measured using Signal Test Setup 3 and Signal Test Setup 6 in Figure 7. The beam power transmitted through the fused silica windows were compared with the beam power incident directly on the transmission detector. The transmission through the fused silica windows and the transparent paraffin blend model diesel was determined to be 0.94 ± 0.01.

The final optical element to be investigated was the final mirror that was employed to reflect the transmitted diode laser beam onto the transmission laser power meter. Twelve different

values for the diode laser attenuation were employed in this calibration. The calibration was conducted using two geometries. In the first geometry, the transmission power detector was placed in the direct path of the incident laser, while in the second geometry, the mirror was placed so that the incident diode laser beam was reflected 90°, onto the transmission detector as shown in Figures 3 and 8.
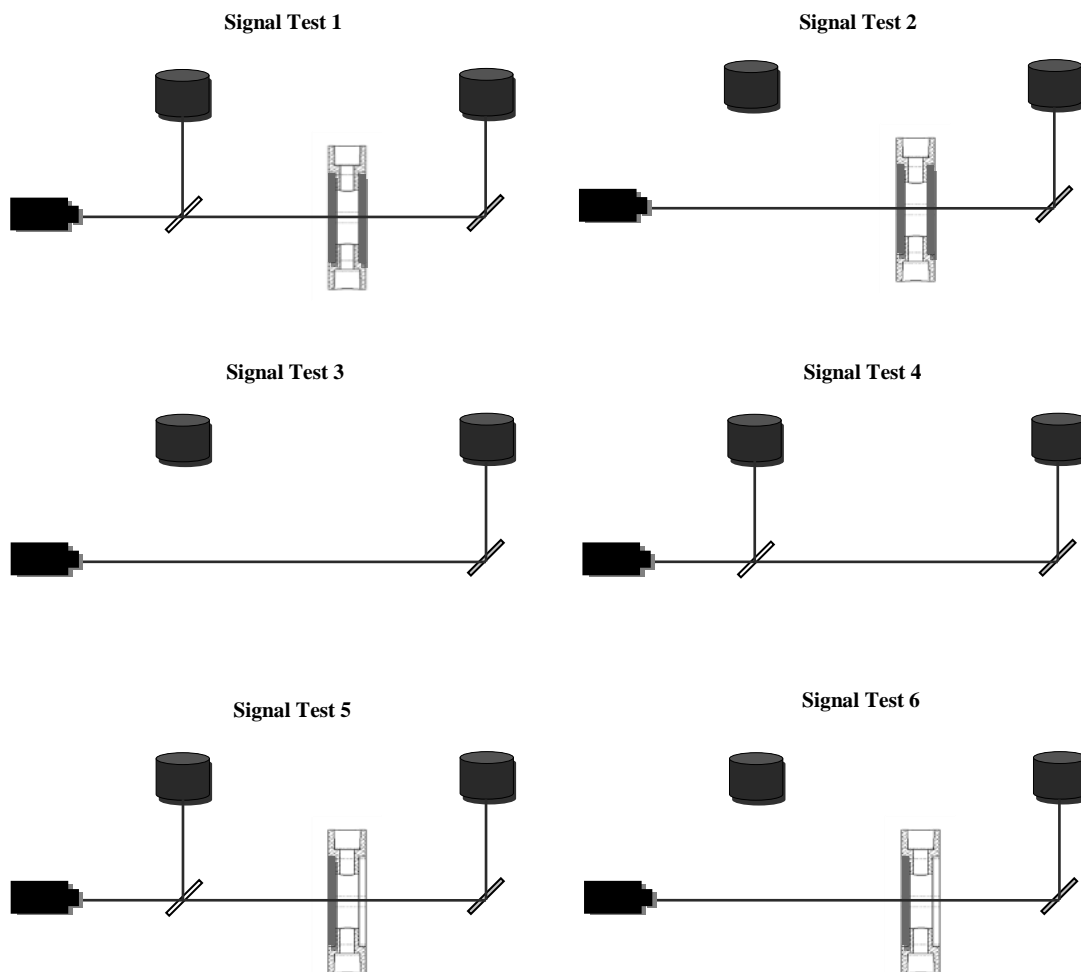

Figure 8: Optical Layout for the Measurement of Reflectivity of Final Mirror

The laser power incident on the mirror was varied by employing a number of different optical elements and neutral density filters, producing a range of different attenuation factors. The

graph of reflected laser power as a function of incident laser power is shown in Figure 9. The final mirror was determined to reflect 0.871 ± 0.007 of the incident laser power.
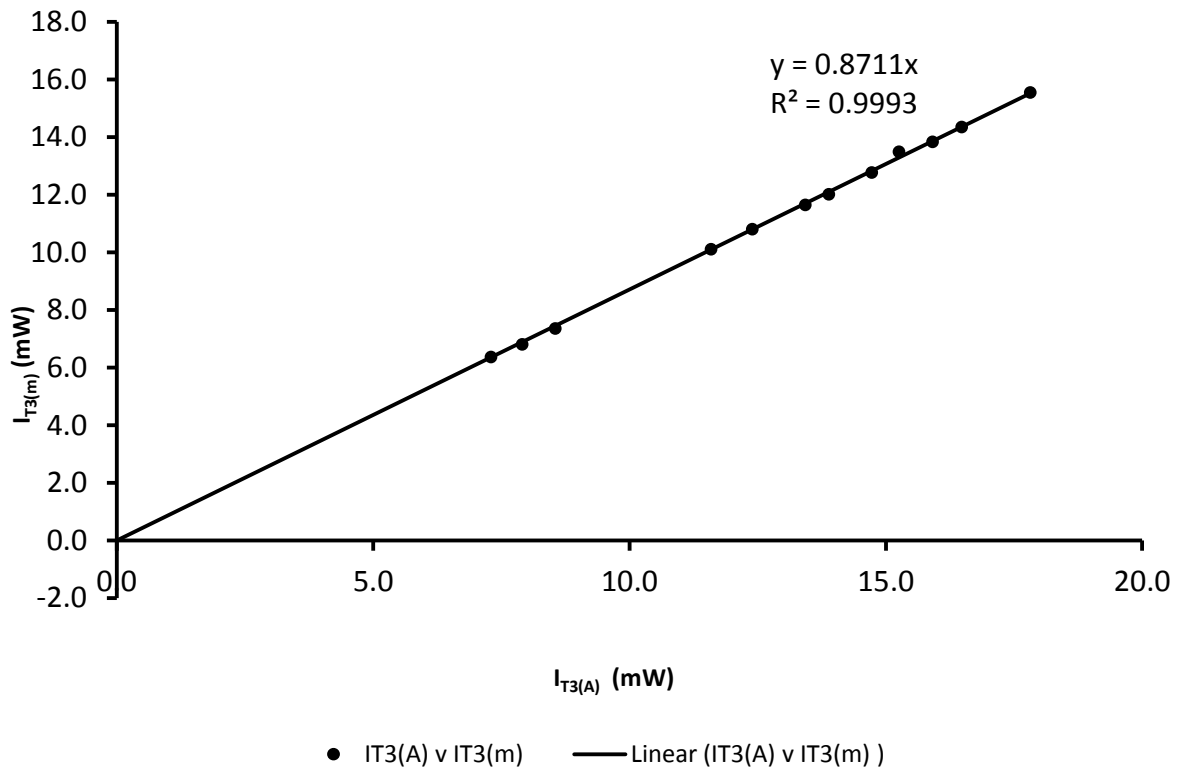

Figure 9: Graph of Reflected Beam Power (mW) from Final Mirror as a Function of Beam Power (mW)

4. Data Analysis

The one-minute averaged laser power measurements for the diesel samples that were subjected to cavitation flow tests were converted to fifteen-minute averages. The continuous fifteen-minute averaged laser transmission power data, were ratioed against the synchronous reference laser power data, producing normalised transmission power data that were independent of power fluctuations in the source 405 nm diode laser.

Figure 10 shows a graph of five normalised transmission laser power to reference laser power profiles as a function of time during the forty hour cavitation test period. The five profiles are identified as fresh commercial diesel samples A and B, aged commercial diesel samples C and D, and the paraffinic rich model diesel sample E. Model diesel E was a blend of C_{10} to C_{19} paraffins, which was almost transparent to the 405 nm laser light. Commercial diesel samples A, B, C and D begin with different extinction coefficients, which is why the normalised values at the beginning of the cavitation tests are different.
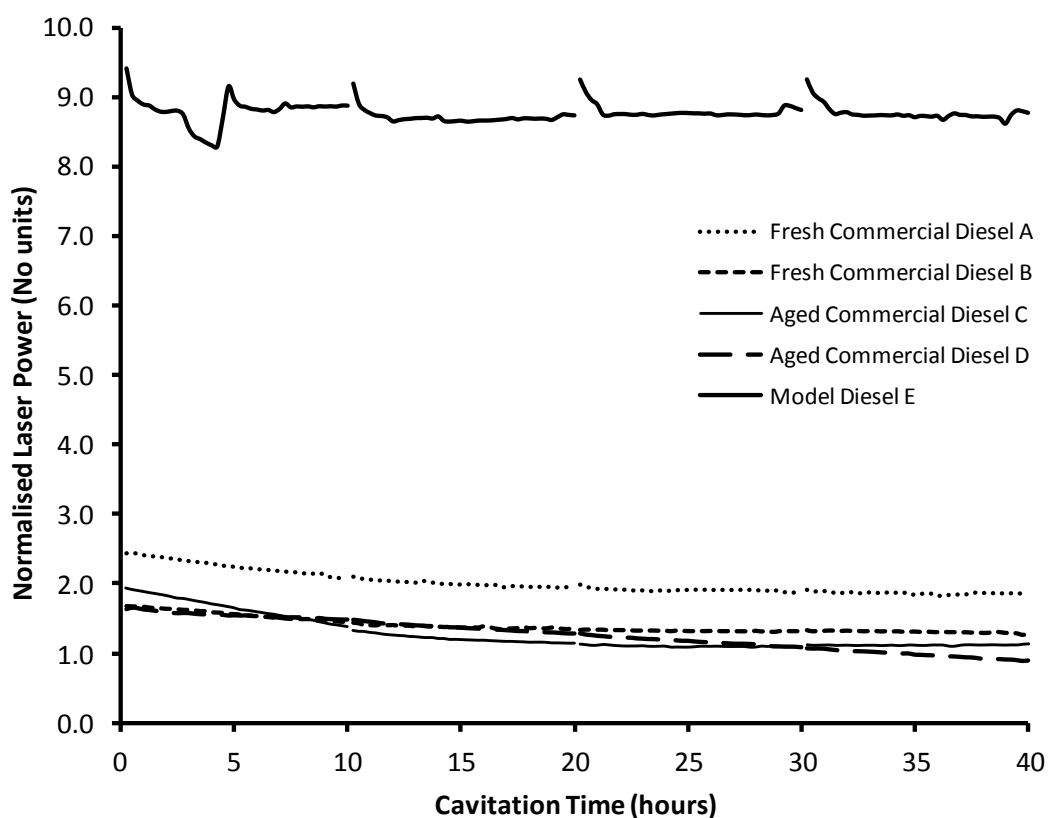

Figure 10: Normalised Transmitted Laser Power as a Function of Cavitation Time (hours) for Three Commercial Diesel Samples and a Paraffin-based Model Diesel.

The time-dependent reflection and transmission laser power measurement data were then employed to determine the time-dependent spectral extinction coefficients for the four

29

commercial diesel samples, together with the samples subjected to immersion in the hot water bath. These were derived using Equation (7).

5. Results

Figure 10 shows a graph of the normalised laser power transmitted through the optical cell containing a 1.03 cm thick layer of commercial or model diesel flowing upward through the cell, as a function of cavitation time (hours) for the forty hour period of the test. The initial extinction coefficient was different for the five diesel fuel samples. The paraffin based model diesel was almost transparent to the incident laser light at 405 nm. In addition, the model diesel extinction coefficient was observed to remain unchanged over the forty hour period of the cavitation flow test.

The relative variation in laser transmission through the respective diesel samples as a function of cavitation test time were determined by normalising the transmission profiles with the corresponding transmission laser power at the beginning of the cavitation tests. These normalised transmission laser power profiles are shown in Figure 11.

The time-dependent variation in the spectral extinction coefficients of the five diesel samples was determined using Equation (7). The results for the five samples were plotted together on the same graph, which is presented in Figure 12.

Figures 13 to 15 show the extinction coefficients derived from the two fresh commercial diesel samples and one of the two aged diesel samples, plotted together with the extinction coefficients derived before and after forty hours immersion in the hot water bath.
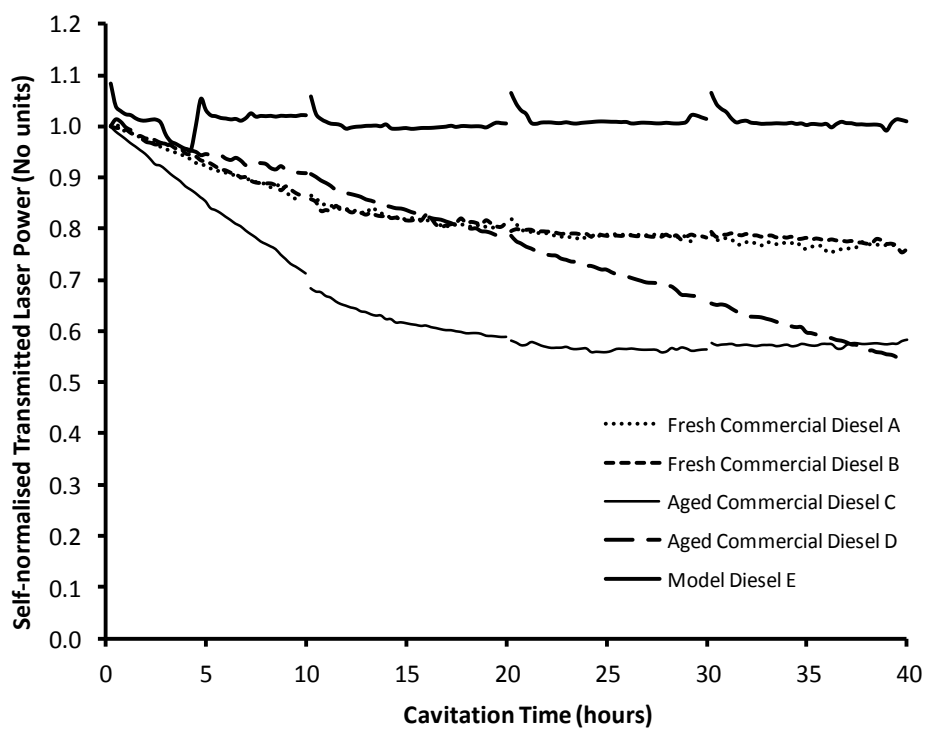
Figure 11: Self-normalised Transmitted Laser Power as a Function of Cavitation Time (hours) for Three Commercial Diesel Samples and a Paraffin-based Model Diesel.
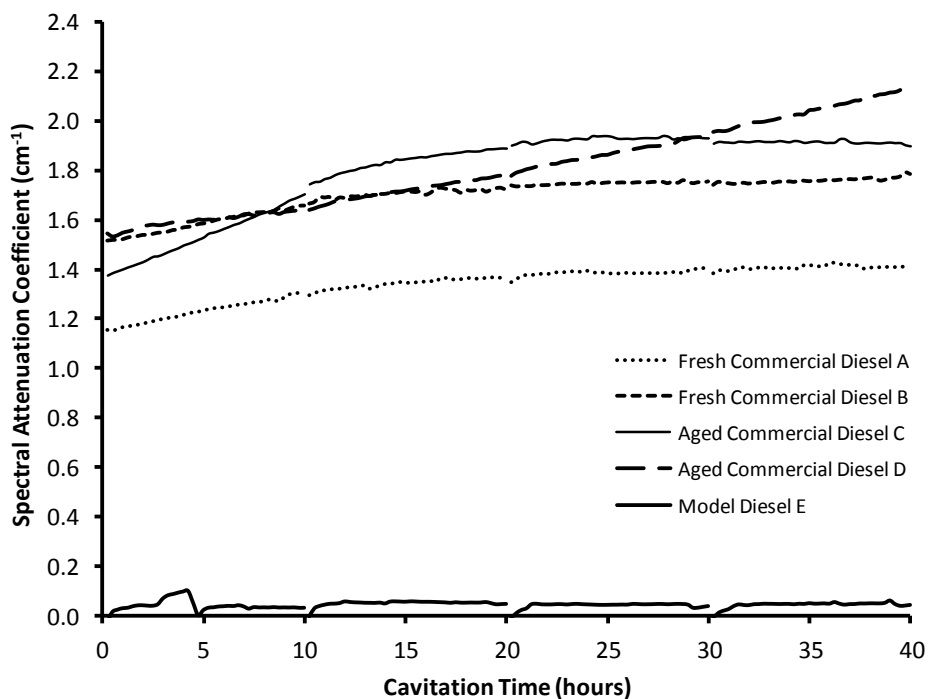

Figure 12: The Spectral Extinction Coefficient (cm^{-1}) as a Function of Cavitation Time (hours) for Three Commercial Diesel Samples and a Paraffin-based Model Diesel.

Figure 13: Graph of the Spectral Extinction Coefficient (cm^{-1}) of: (a) Cavitated Sample A, (b) Reference Sample A, and (c) Heated Sample A, as a Function of Cavitation Time (hours).

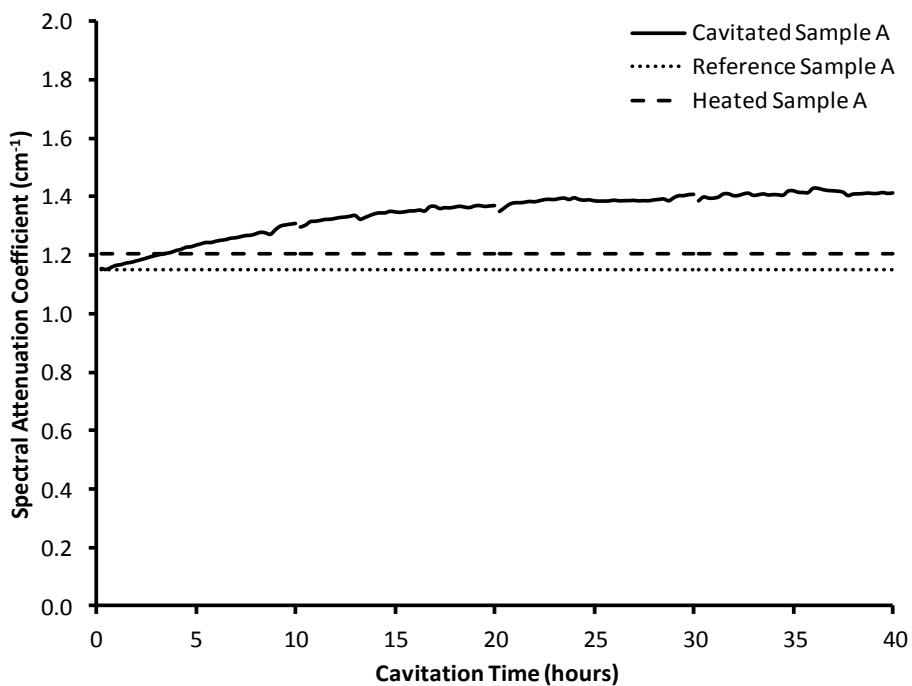**Figure 14: Graph of the Spectral Extinction Coefficient (cm^{-1}) of: (a) Cavitated Sample B, (b) Reference Sample B, and (c) Heated Sample B, as a Function of Cavitation Time (hours).**

32

Figure 15: Graph of the Spectral Extinction Coefficient (cm^{-1}) of: (a) Cavitated Sample C, (b) Reference Sample C, and (c) Heated Sample C, as a Function of Cavitation Time (hours).
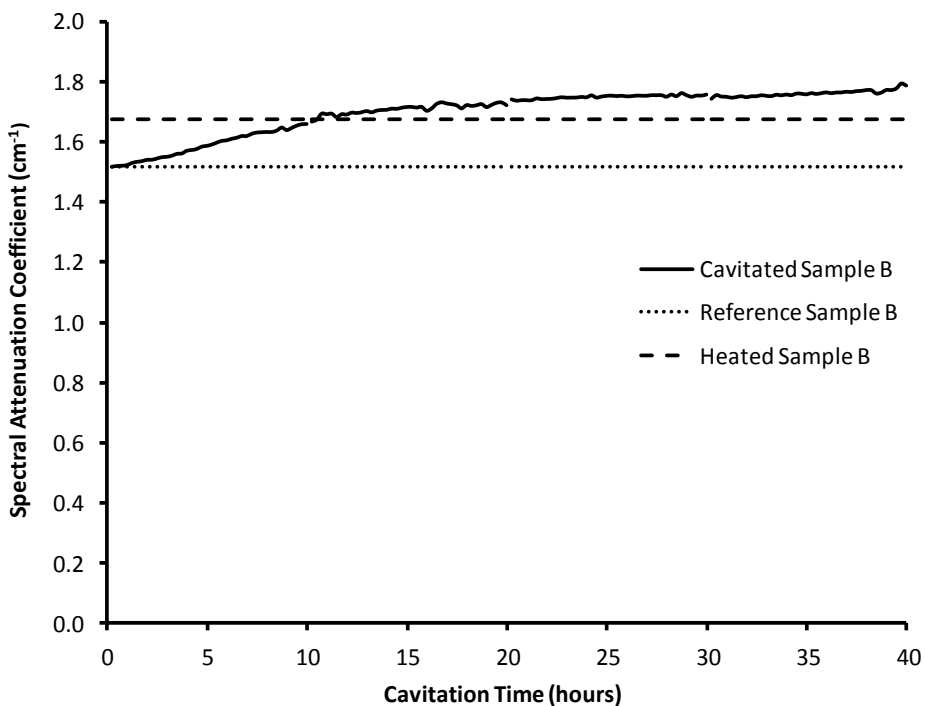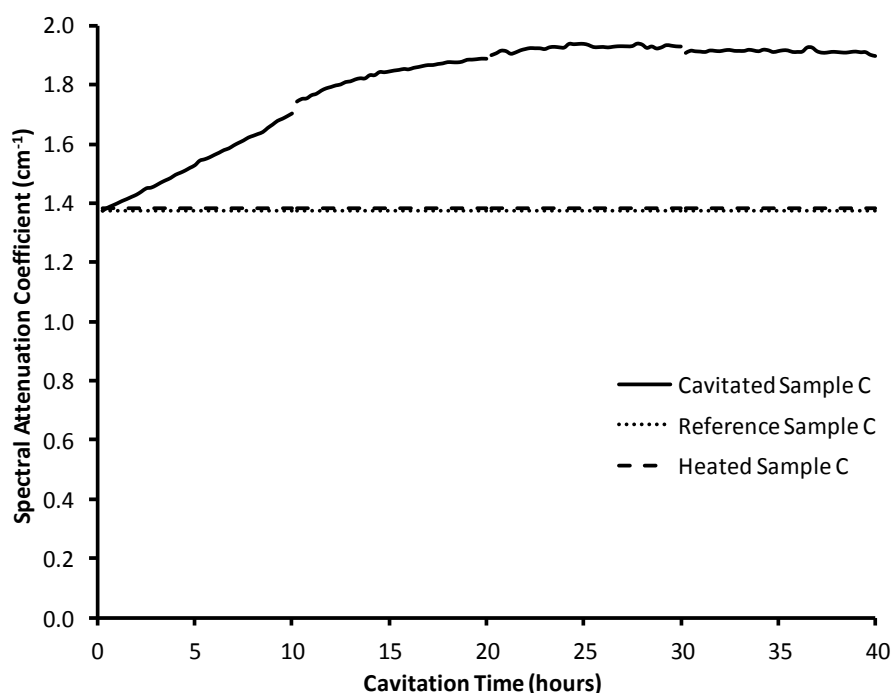
6. Discussion

6.1 Variations in Spectral Extinction Coefficients

Figure 10 shows the transmitted laser power normalised by the reference laser power for two fresh commercial diesel samples, and two aged commercial diesel samples, together with a paraffin-blend model diesel, plotted against the cavitation time that the samples were subjected to. The paraffin blend model diesel is almost transparent to the 405 nm laser light, and shows negligible change in absorption over the forty hour cavitation period. In contrast to this, all of the commercial diesel samples produce a decrease in normalised laser transmission power with time during the cavitation.

33

The scale of the decrease in normalised transmission power can be observed in Figure 11, which shows the relative change in normalised laser transmission power through the four commercial diesel samples and the paraffin-blend model diesel sample. The paraffin-blend model diesel produces very little change in the normalised transmitted laser power over the forty hour cavitation period. By contrast, the two fresh commercial diesel samples produce a very similar relative decrease in normalised transmitted laser power, decreasing approximately 22 % from the initial value over the forty hour period. The aged samples were observed to produce an even greater decrease in transmitted laser power, decreasing approximately 40% from the initial value after the forty hour cavitation period. It is important to note however, that the aged samples produced very different laser transmission histories. Aged diesel sample C produced a profile which decreased rapidly after cavitation began, and levelled out in the middle to late period. In contrast, aged diesel sample D produced a linearly decreasing transmission profile.

Equation (7) was employed to calculate the spectral extinction coefficients for all of the diesel samples as a function of the cavitation time. The results of these calculations are shown in Figure 12. The paraffin-blend model diesel was revealed to have an unchanged 405 nm spectral extinction coefficient of 0.05 cm^{-1} $\pm$ 0.03 cm^{-1} during the cavitation period. Fresh commercial diesel sample A began with an initial 405 nm spectral extinction coefficient of 1.15 cm^{-1} $\pm$ 0.02 cm^{-1}, increasing to 1.42 cm^{-1} $\pm$ 0.02 cm^{-1} at the end of the forty hour cavitation period. Fresh commercial diesel sample B began with an initial spectral extinction coefficient of 1.52 cm^{-1} $\pm$ 0.02 cm^{-1}, increasing to 1.79 cm^{-1} $\pm$ 0.02 cm^{-1} over the forty hour cavitation period. Aged commercial diesel samples C and D began with initial spectral extinction coefficients of 1.38 cm^{-1} $\pm$ 0.02 cm^{-1} and 1.53 cm^{-1} $\pm$ 0.02 cm^{-1}

respectively, increasing to 1.90 cm^{-1} ± 0.02 cm^{-1} and 2.13 cm^{-1} ± 0.02 cm^{-1} respectively over the forty hour cavitation period.

Three of the four commercial diesel samples (fresh samples A and B, and aged sample C) were subjected to discontinuous heating in a modified water urn at 70 ^{o}C ± 1 ^{o}C for forty hours, mimicking the forty hour cavitation period. This was done in order to separate out the effects of temperature and cavitation flow in changing the spectral extinction coefficients over the forty hour cavitation period.

Figure 13 shows the graph of the variation of spectral extinction coefficient with cavitation time for fresh diesel sample A, together with the corresponding spectral extinction coefficients for sample A obtained before and after forty hours discontinuous immersion in the water bath. The discontinuous immersion of sample A in the water bath for forty hours produces a 4.5 % change in the spectral extinction coefficient, compared with the 24 % increase that occurred as a result of the forty hours cavitation flow. This means that the cavitation flow is responsible for a 19.5 % increase in the spectral extinction coefficient over the forty hour cavitation period.

Figure 14 shows the graph of the variation of spectral extinction coefficient with cavitation time for fresh diesel sample B, together with the corresponding spectral extinction coefficients for sample B obtained before and after forty hours discontinuous immersion in the water bath. The discontinuous immersion of sample B in the water bath for forty hours produces a 10.5 % change in the spectral extinction coefficient, compared with the 18 % increase that occurred as a result of the forty hours cavitation flow. This means that the cavitation flow is responsible for an 7.5 % increase in the spectral extinction coefficient over

the forty hour cavitation period. A comparison of the respective effects of the immersion of fresh diesel samples A and B in the water bath shows that temperature produced a more significant change in the spectral extinction coefficient for sample B relative to sample A.

Figure 15 shows the graph of the variation of spectral extinction coefficient with cavitation time for aged diesel sample C, together with the corresponding spectral extinction coefficients for sample C obtained before and after forty hours discontinuous immersion in the water bath. The discontinuous immersion of sample C in the water bath for forty hours produces a 0.8 % change in the spectral extinction coefficient, compared with the 40.5 % increase that occurred as a result of the forty hours cavitation flow. This means that the cavitation flow is responsible for a 38 % increase in the spectral extinction coefficient over the forty hour cavitation period. It appears that the immersion of aged diesel sample C in the water bath had very little effect on the spectral extinction coefficient.

The composition of modern crude-oil derived diesel is approximately 72 % paraffins, 22 % mono-aromatics, 3 % di-aromatics, and 1 % tri-aromatics [39]. Considering that the paraffinic-rich model diesel was comprised principally of C_{10} to C_{19} paraffins (> 98 %), and that the forty hour cavitation period had no measureable effect on the 405 nm spectral extinction coefficient, suggests that any chemical changes to the composition of the model diesel during cavitation had no measureable effect on its overall spectral extinction coefficient.

This conclusion leads to the suggestion that the observed variations in the 405 nm spectral extinction coefficients as a function of cavitation time for the fresh and aged commercial diesel samples have been caused by changes to the aromatic content in the commercial diesel

samples. Noting the propensity for simple aromatics to form complex polycyclic aromatic hydrocarbons (PAHs), leading to the formation of small soot-like particles suggests the hypothesis that the increase in spectral extinction coefficients with cavitation time for the commercial diesels was caused by the aromatics comprising the diesel undergoing pyrolysis-like reactions during cavitation to form a particle suspension, hence increasing the optical extinction coefficients of the cavitated samples.

This hypothesis would also explain why the aged diesel samples both produced larger relative variations in their respective spectral extinction coefficients than those produced from the fresh diesel samples. The aged diesel samples would have been more susceptible to aromatic pyrolysis to form particles than the fresh commercial diesel samples, due to their reduced fuel stability as a result of long-term storage [25, 26].

A note of caution is necessary. The increases in spectral extinction coefficients are common to all of the commercial diesel fuel samples subjected to cavitation flow. However, all of the commercial diesel fuel samples tested will have contained an unknown concentration and composition of additives, surfactants and detergents (normally less than 1% vol/vol), which would have had an unpredictable effect on the spectral extinction coefficients of the tested diesel fuel samples. However, the consistent increase in spectral extinction coefficients common to all of the samples tested suggests that sono-chemical alterations to the fuel components common to the commercial diesel samples were responsible. These common fuel components present in all of the commercial diesel samples were dominated by the mono-aromatics.

6.2 Particulate Formation and Volumetric Flow Rate

The volumetric flow rate of the diesel fuel samples through the cavitation flow rig was estimated to be approximately 3.2 l/min ± 0.3 l/min, when the rig was operated at 550 bar pressure and 1,500 rpm, with the diesel temperature maintained at 70 ^{o}C. This estimate was derived from the predicted mass flow rate based on the Bernoulli velocity, together with an estimated discharge coefficient of 0.77 ± 0.05 (which is typical of diesel nozzles at approximately 550 bar pressure [1]).   This estimated fuel volume flow rate was also consistent with the specification flow rate curve supplied for the Dynex PF1318H-10 pump [37].

The cavitation flow rig supported a fuel sample volume of 3.5 litres. A volumetric flow rate of 3.2 l/min circulated the entire 3.5 l volume of the diesel fuel samples in approximately 1.1 minutes, leading to a fuel sample cavitation recycling rate of approximately 55 ± 5 cycles/hour, and approximately 2,200 ± 200 complete cavitation cycles over forty hours. In comparison, a modern passenger car common rail diesel pump is capable of supporting a volumetric flow rate of approximately 1.4 l/min continuously at 550 bar rail pressure, a volumetric flow rate of approximately 0.8 l/min continuously at 1,650 bar rail pressure [1], and an instantaneous volumetric flow rate of approximately 30 l/min during discrete fuel injection into an engine (based on an approximate maximum of 0.6 cm^3 injected fuel volume per injection cycle).

If the mean diesel fuel return rate from the pump, common rail and injectors back to the tank is estimated to be approximately 35 % of the fuel supplied from the common rail, then the volumetric flow rate of high pressure diesel fuel returned to the tank may be as much as 0.3

l/min. The results presented here suggest that deposits and/or sediments produced by cavitation occurring inside the pump and at the entrance to the injectors may be observable after the pump has pumped approximately 20,000 litres of diesel fuel. This corresponds to a mean passenger vehicle mileage of approximately 200,000 km. However, there is additional evidence to suggest that the rate of formation of particulates as a result of cavitation pyrolysis is proportional to the square of the rail pressure [1]. This means that fuel deposits and/or sediments may be detectable in the fuel injection equipment after approximately 5,000 litres of fuel has been pumped to mean rail pressures of approximately 1,100 bar (corresponding to a vehicle mileage of approximately 40,000 km).

In contrast to this, a typical large, transportation truck (30 ton - 40 ton carrying capacity), employing a six-/eight-cylinder 12 litre/16 litre engine, capable of 450 kW to 550 kW of brake power output, has a typical fuel consumption of 30 l/100 km to 35 l/100 km. The common rail pumps used in these engines are believed to be capable of supplying diesel to the engine at an approximate rate of 4.5 l/min continuously at 2,000 bar rail pressure. This suggests that the fuel return rate may be as much as 1.5 l/ min back to the tank, assuming a mean fuel return of approximately 30 % to 35 %.

As before, the engine may begin to show the effects of high pressure pumping cavitation after pumping approximately 20,000 litres of diesel fuel. This corresponds to an average heavy goods vehicle distance of approximately 45,000 km to 50,000 km. However, taking the suggested dependence of the particulate formation rate on common rail pressure into account, suggests that fuel deposits and/or sediments may be detectable in the fuel injection equipment after the high pressure pumping of approximately 5,000 litres of diesel (corresponding to a vehicle mileage of approximately 11,000 km to 12,000 km).

7. Conclusion

A novel recirculation, continuous cavitation flow rig has been designed and manufactured in order to test the effect of high pressure cavitation flow on the chemical stability of diesel fuels. The change in composition and/or stability of the fuel was determined through the continuous measurement of the spectral extinction coefficients of the cavitated diesel samples at 405 nm as a function of the cavitation time.

A commercial tea urn was modified in order to immerse diesel samples in heated water, in order to mimic the temperature history of the diesel samples in the cavitation flow rig. This was done in order to separate the effect of temperature from the effect of cavitation on the diesel samples.

Five diesel samples were tested in the cavitation flow rig and immersion in the water bath. These samples consisted of two fresh commercial diesels that were subjected to cavitation flow testing within three months of purchase, two aged commercial diesel samples that were stored in a fuel store for twelve to fifteen months, and then subjected to cavitation flow testing and immersion in the water bath, and a model diesel comprised of a C_{12} to C_{19} paraffin blend.

The model diesel produced almost no variation in spectral extinction coefficient, and hence almost no variation in spectral absorption and scattering during and after the forty hour cavitation period. This suggests that any variation that occurred in the composition of the model diesel sample during cavitation had a negligible effect on the spectral extinction coefficient of the model diesel sample.

In contrast, the fresh commercial diesel samples were observed to undergo a continuous increase in spectral extinction coefficients during cavitation flow, leading to a 20 % to 25 % increase in spectral extinction over forty hours. The aged commercial diesel samples were observed to undergo an even greater increase in spectral extinction during the cavitation period, leading to a 40 % to 50 % increase in spectral extinction coefficient after forty hours cavitation.

Approximately 80 % of the increase in the spectral extinction coefficient of fresh commercial diesel sample A was attributed to the effect of cavitation, and the balance (20 %) was attributed to the effect of temperature. In contrast, approximately 45% of the increase in the spectral extinction coefficient of fresh commercial diesel sample B was attributed to the effect of cavitation, and the balance (55 %) was attributed to the effect of temperature. Approximately 99 % of the increase in the spectral extinction coefficient of aged commercial diesel sample C was attributed to the effect of cavitation, and the balance (1 %) attributed to the effect of temperature.

A comparison of the composition of the paraffin-rich model diesel, together with the absence of variation in spectral extinction during cavitation, with the composition of the commercial diesels and the consistent increase in the spectral extinction coefficients of these samples during cavitation, leads to the conclusion that the cavitation affected the aromatics in the commercial diesels. It is likely that the aromatics were undergoing pyrolysis-like reactions during cavitation to form complex polycyclic aromatic hydrocarbons (PAHs), and even small particles in suspension. This hypothesis would explain the relative increase in the spectral extinction produced by the aged diesel samples (C and D) when compared with that produced

41

by the fresh commercial diesel samples (A and B), in terms of the reduced chemical stability of the aged samples when compared with the fresh samples.

References

1. R.D. Lockett, M. Jeshani, to be published (2013).

2. G. Lepperhof, M. Houben, Mechanisms of Deposit Formation in Internal Combustion Engines and Heat Exchangers, SAE Technical Paper 931032 (1993) doi:10.4271/931032.

3. J. Tang, S. Pischinger, M. Lamping, T. Korfer, M. Tutur, D. Tomazic, Coking Phenomena in Nozzle Orifices of DI-Diesel Engines, SAE International Journal of Fuels and Lubricants 2:1 (2009) 259 - 272. doi:10:4271/2009-01-0837.

4. J. Ullman, M. Geduldig, H. Stutzenberger, R. Caprotti, G. Balfour, Investigation into the Formation and Prevention of Internal Diesel Injector Deposits, SAE Technical Paper 2008-01-0926 (2008).

5. S. Pehan, M.S. Jerman, M. Kegl, B. Kegl, Biodiesel influence on tribology characteristics of a diesel engine, Fuel 88:6 (2009) 970 - 979.

6. R. Caprotti, A. Breakspear, O. Graupner, T. Klaua, O. Kohnen, Diesel Injector Deposits Potential in Future Fuelling Systems, SAE Technical Paper 2006-01-3359 (2006).

7. Y.M. Arafin, T. Furuhata, M. Saito, M. Arai, Diesel and bio-diesel fuel deposits on a hot surface, Fuel 87: 8-9 (2008) 1601 - 1609.

8. Y.M. Arafin, M. Arai, The effect of hot surface temperature on diesel fuel deposit formation, Fuel 89:5 (2010) 934 - 942.

9. C. Soteriou, R. Andrews, M. Smith, Direct injection diesel sprays and the effect of cavitation and hydraulic flip on atomization, SAE paper 950080 (1995).

10. F. Payri, V. Bermudez, R. Payri, F.J. Salvador, The influence of cavitation on the internal flow and the spray characteristics in diesel injection nozzles. Fuel 83 (2004) 419 – 431.

11. A. Andriotis, M. Gavaises, C. Arcoumanis, Vortex flow and cavitation in diesel injector nozzles, Journal of Fluid Mechanics 610 (2008) 195–215.

12. Badock C, Wirth R, Tropea C. The influence of hydro grinding on cavitation inside a diesel injection nozzle and primary break-up under unsteady pressure conditions. In: Proceedings of the ILASS-EUROPE. Toulouse, France; 1999.

13. A. Osman, Failure of a diesel engine injector nozzle by cavitation damage, Engineering Failure Analysis 13:7 (2006) 1126 – 1133.

14. H. Roth, M. Gavaises, C. Arcoumanis, Cavitation initiation, its development, and link with flow turbulence in diesel injector nozzles. SAE paper 2002-01-0214 (2002).

15. H. Roth, Experimental and computational investigation of cavitation in diesel injector nozzles, PhD thesis, Imperial College, London, UK, (2004).

16. R.D. Lockett, L. Liverani, D. Thaker, M. Jeshani, N.P. Tait, The characterisation of diesel nozzle flow using high speed imaging of elastic light scattering, Fuel 106 (2013) 605 - 616.

17. Y. He, Z. Zhao, J. Liu, H. Du, M.Li, Y. Zong, Two-phase flow of liquid-gas in diesel fuel injection system and their effect on engine performances, Journal of Thermal Sciences 10:3, (2001) 223 - 227.

18. R. Price, D. Doyle, Private Communication, Shell Global Solutions (2012).

19. Diesel Systems: Common Rail Systems CRSN3 with 2,000 to 2,500 bar, Robert Bosch GmbH Diesel Systems, http://www.bosch-kraftfahrzeugtechnik.de/media/db_application/downloads/pdf/antrieb/en_3/DS_Sheet_CRSN3_with_2_000_to_2_500_bar_20120730~3.pdf

20. Y. Shinohara, K. Takeuchi, O.E. Herrmann, H.J. Laumen, 3000 bar Common Rail System, MTZ Worldwide Magazine 72:1, ISSN 2192-9114, Springer Automotive Media (2011) 4 - 9. DOI: 10.1365/s38313-011-0002-8

21. M. Graham, N. Keeler, J. Kewley, Ultra-high pressure common rail systems, IMechE Conf. Injection Systems for IC Engines, London, ISBN 9781843345619 (2009) 231 - 243.

22. K.S. Suslick, J.J. Gawienowski, P.F. Schubert, H.H. Wang, Alkane sonochemistry, Journal of Physical Chemistry 87: 13 (1983) 2299 - 2301.

23. G.J. Price, M. McCollom, The effect of high-intensity ultrasound on diesel fuels, Ultrasonics Sonochemistry 2: 2 (1995) S67 - S70.

24. G.J. Price, M. McCollom, Use of high-intensity ultrasound as a potential test method for diesel fuel stability, Fuel 74: 9 (1995) 1394 - 1397.

25. J.F. Pedley, R.W. Wiley, R.A. Hancock, Storage stability of petroleum-derived diesel fuel 3: Identification of compounds involved in sediment formation, Fuel 67:8 (1988) 1124 - 1130.

26. Z.D. Kalitchin, S.K. Ivanov, M.I. Boneva, P.T. Georgiev, A. Ivanov, K. Kanariev, Chemical stability of diesel fuels and sediment formation therein: 1. Evaluation of the chemical stability of diesel fuels by following the kinetics of sediment formation, Fuel 71: 4 (1992) 437 - 442.

27. Ultrasonics Sonochemistry, Elsevier Journals, ISSN 1350-4177, Reed-Elsevier.

28. D.J. Flannigan, K.S. Suslick, Plasma formation and temperature measurement during single-bubble cavitation, Nature 434 (2005) 52 - 55.

29. K.S. Suslick, D.J. Flannigan, Inside a Collapsing Bubble: Sonoluminescence and the Conditions During Cavitation, Annual Reviews of Physical Chemistry 59 (2008) 659 - 683.

30. H. Richter, J.B. Howard, Formation of polycyclic aromatic hydrocarbons and their growth to soot - a review of chemical reaction pathways, Progress in Energy and Combustion Science 26 (2000) 565 - 608.

31. A.R. Jones, Light scattering for particle characterization, Progress in Energy and Combustion Science 25 (1999) 1 - 53.

32. I.T. Horvath, M.R. Vetrano, Development of the Multi Wavelength Light Extinction Technique for the Characterization of Nanoparticles - Data Inversion, 9th national Congress on Theoretical and Applied Mechanics, Brussels, May 2012.

33. L.B. Scaffardi, N. Pelligri, O. de Sanctis, J.O. Tocho, Sizing gold nanoparticles by optical extinction spectroscopy, Nanotechnology 16:1 (2005) 158.

34. G. Yamamoto, M. Tanaka, Determination of aerosol size distribution from spectral attenuation measurements, Applied Optics 8:2 (1969) 447 - 453.

35. F.E. Hoge, Laser measurement of the spectral extinction coefficients of fluorescent, highly absorbing liquids, Applied Optics 21:10 (1982) 1725 - 1729.

36. W. Leupacher, A. Penzkofer, Refractive-index measurement of absorbing condensed media, Applied Optics 23:10 (1984) 1554 - 1558.

37. Dynex Engineering Specifications, Checkball Piston Pumps, PF1300 Series, http://www.dynexhydraulics.com/dynexpf1300specs.pdf

38. C.F. Bohren, D.R. Huffman, Absorption and Scattering of Light by Small Particles, Wiley-VCH Verlag GmbH & Company (2004) ISBN 0-471-29340-7.

39. J. Erwin, Assay of Diesel Fuel Components Properties and Performance, Symposium on Processing and Product Selectivity of Synthetic Fuels, Division of Fuel Chemistry, American Chemical Society, Washington DC, USA, 23 - 28 August, 1992.

Acknowledgements

Table 1: Comparison of Beam Power with and without Final Mirror Using Three Beam Splitters

Signal Test No.	Splitter 1		Splitter 2		Splitter 3	
	Actual Setup Test Results-$I_{T3(m)}$ **(y)**	No Mirror Setup Test Results-$I_{T3(A)}$ **(x)**	Actual Setup Test Results-$I_{T3(m)}$ **(y)**	No Mirror Setup Test Results-$I_{T3(A)}$ **(x)**	Actual Setup Test Results-$I_{T3(m)}$ **(y)**	No Mirror Setup Test Results-$I_{T3(A)}$ **(x)**
1	12.0195	13.8875	10.112	11.59	6.3705	7.297
2	13.4955	15.25619048	-	-	-	-
3	15.553125	17.817	-	-	-	-
4	13.8395	15.911	11.651	13.4285	7.3605	8.551
5	12.775	14.7245	10.8075	12.3945	6.8095	7.9055
6	14.354	16.4795	-	-	-	-